Nuclear magnetic and conductivity relaxations by Li diffusion in glassy and crystalline LiAlSi 4O 10

ARTICLE *in* JOURNAL OF NON-CRYSTALLINE SOLIDS · JUNE 1997

Impact Factor: 1.77 · DOI: 10.1016/S0022-3093(96)00654-0

3 AUTHORS, INCLUDING:

Paul Heitjans
Leibniz Universität Hannover
265 PUBLICATIONS **3,613** CITATIONS

ELSEVIER

Journal of Non-Crystalline Solids 212 (1997) 215–224

JOURNAL OF NON-CRYSTALLINE SOLIDS

Nuclear magnetic and conductivity relaxations by Li diffusion in glassy and crystalline $LiAlSi_4O_{10}$

R. Winter, K. Siegmund, P. Heitjans *

Institut für Physikalische Chemie und Elektrochemie and Sonderforschungsbereich 173, Universität Hannover, Callinstraße 3-3A, 30167 Hannover, Germany

Received 22 July 1996; revised 11 November 1996

Abstract

The dependence of lithium diffusion on the degree of structural order was investigated in $LiAlSi_4O_{10}$ in its glassy and polycrystalline states by nuclear magnetic resonance (NMR) and ionic conductivity relaxation techniques. The NMR measurements were performed in the temperature range from 150 K to 1000 K, which covers the diffusion induced spin–lattice relaxation rate (T_1^{-1}) maximum for each of the modifications. The dependence of T_1^{-1} on the Larmor frequency was observed in the range from 11.3 MHz to 38.9 MHz. Impedance spectroscopy was carried out on the glassy sample in the frequency interval from 100 Hz to 10 MHz and for temperatures between ambient temperature and 670 K. The results obtained from the two methods reflect significant deviations of the relaxation processes from their respective standard models (BPP and Debye) with regard to anomalous frequency dependences of T_1^{-1} and of the conductivity, and a difference between the low and high temperature activation energies. These anomalies are discussed in terms of the dynamic structure model and other theories for anomalous relaxation in ionic conductors. When the results are analyzed in the framework of the dynamic structure model there are indications for clustering of the mobile species which results in correlated motion of Li ions. In a crystalline sample, the activation energy is larger and the jump frequency is smaller than in the amorphous material.

PACS: 76.60.Es; 61.43.Fs; 66.30.Hs; 61.72.Ji

1. Introduction

Lithiumalumosilicates belong to a group of compounds which can be utilized to create tailored materials with well-defined physical properties. In the special case of the Li_2O–Al_2O_3–$nSiO_2$ compounds it is easy to manipulate the thermal expansion coefficient by tuning the degree of structural order, i.e., by partial crystallization of the glassy material. The possibility of designing glass-ceramics by this means is due to the fact that the crystalline lithiumalumosilicates have a negative thermal expansion coefficient while their glassy counterparts behave regularly in this respect [1]. These materials are also known to exhibit lithium ionic conductivities of the order of 10^{-7} S m^{-1} at room temperature [2,3]. The objective of the present study is to examine the dependence of ionic motion on the extent of structural order in the two limits of amorphous and polycrystalline material of the same composition $LiAlSi_4O_{10}$

* Corresponding author. Tel.: +49-511 762 3187; fax: +49-511 762 4009; e-mail: heitjans@curie.pci.uni-hannover.de.

PII S0022-3093(96)00654-0

($\triangleq Li_2O \cdot Al_2O_3 \cdot 8SiO_2$ in the system $Li_2O \cdot Al_2O_3$–$nSiO_2$). To this end, both the nuclear magnetic resonance (NMR) technique and impedance spectroscopy (IS) are employed. In the present study, the two methods cover the frequency range from 100 Hz to 40 MHz. While the impedance measurements are restricted to frequencies below 10 MHz, NMR becomes the method of choice at higher frequencies. For future work, a more extensive overlap of the frequency ranges of both methods turns out to be desirable for a more detailed comparison, and its technical realization is in progress.

The structure of polycrystalline $LiAlSi_4O_{10}$ is similar to that of β-spodumene, $LiAlSi_2O_6$ ($n = 4$) [4]. β-spodumene, as well as β-eucryptite, $LiAlSiO_4$ ($n = 2$), has already been studied by this group [3,5] and others [6]. The crystalline sample of the present study is isostructural with β-spodumene except for the decreased Li content, whose charge deficit is balanced by the change of the fraction of silicon atoms in the Al–Si sublattice [7]. Consequently a direct comparison of these two crystalline materials is possible with respect to the mobile charge carrier concentration.

2. Experimental

2.1. Sample preparation

The glassy sample, prepared by rapid roller quenching [8], was supplied by Schott Glaswerke, Mainz. Chemical analysis by means of optical emission spectral analysis with inductively coupled plasma (ICP-OES) proved the sample to have stoichiometric composition; the deviation from the expected mass proportions is 2.3% at most. The concentration of paramagnetic impurities was found to be less than the experimental accuracy of 75 ppm. Because of the high purity of the sample also with respect to other alkali elements than lithium, a decrease of the conductivity values due to the mixed alkali effect may not be expected.

In order to exclude the glass transition (T_g, as reported in the literature [9], is about 1170 K) in the relevant temperature range, we carried out a differential scanning calorimetry (DSC) measurement from 773 K up to 1043 K. While heating the sample with a rate of 3 K min^{-1} neither exo- nor endothermal peaks occurred, indicating that the glass transition does not take place in this temperature range.

The crystalline sample was prepared by heating the pulverized glass in a platinum crucible in air for 2 weeks at about 820 K. Afterwards it was cooled to room temperature without explicitly quenching it. From the white powder obtained by this procedure diffractometer plots were recorded. The lattice plane distances d obtained from these are consistent with those given by Ostertag et al. [7] for β-spodumene–SiO_2 solid solution. Magic angle spinning (MAS) NMR measurements show different chemical shift values for the glass (−0.84 ppm, versus LiCl aq.) and the crystalline product (−0.36 ppm). According to the product spectrum the sample is free of residual glass within the limits of accuracy.

2.2. NMR — experimental

For the measurement of ^7Li spin–lattice relaxation times, T_1, the samples were placed in boron nitride tubes of 30 mm length and 10 mm diameter; each vessel was closed with two lids which were fixed by use of an alumina-water suspension as glue.

The NMR experiments were carried out using an MR 300 DT spectrometer (Surrey Medical Imaging Systems (SMIS)). The rf pulses were amplified by an ENI LPI-10 pulse amplifier with 1000 W maximum power output. A 2.3 T electromagnet (Bruker) was used with a home-made probe (for details see Ref. [10]) equipped with two inserts for measurements above or below room temperature (except for the 38.9 MHz series, for which we used a field adjustable 7 T cryomagnet (Oxford Instruments) [5]. In the first case heating was by means of a resistance heater controlled by an ITC 4 temperature controller (Oxford Instruments); in the latter case the probe was cooled by a constant stream of vaporized nitrogen, the temperature of which was also adjusted by the ITC 4.

The spectral width in all NMR experiments was 200 kHz. In order to achieve complete destruction of residual magnetization before each single measurement we used a saturation recovery sequence with a saturation comb comprising 10 pulses ($10 \times \pi/2 - \tau - \pi/2$-sequence). The $\pi/2$ pulse width varied, dependent on temperature and frequency conditions, from 4.2 μs to 6.0 μs. The NMR experiments covered the temperature range 150 K $< T <$ 960 K

for the glassy and 300 K $< T <$ 1000 K for the crystalline sample. In the glassy specimen the frequency dependence of the spin–lattice relaxation rate was investigated at five different Larmor frequencies in the range 11.3 MHz $< \nu_0 <$ 38.9 MHz, while the crystalline material was examined, in order to compare both modifications, at one frequency (24.5 MHz) only.

As will be shown later, the relaxation in $LiAlSi_4O_{10}$ is mainly due to quadrupolar interaction. Nevertheless, a single exponential function fits the time evolution of the ^7Li nuclear magnetization in case of the crystal very well. In the glassy material some deviation from this fit is observed which, however, is 15% at most, and a single exponential may be used here as well in order to permit comparisons.

2.3. IS — experimental

Pieces of glass with parallel surfaces were polished to a thickness of 200 μm. This results in cell constants of the four samples in the range from 19 cm to 70 cm. It was difficult to find a material for the electrodes which adheres well to the glass with good electrical contact. A paintable graphite dispersion turned out to be the best material. Although the uncertainty of the cell constant is in the order of 10%, this will not affect the temperature and frequency dependences of the conductivity but only its absolute value. Apart from polarization of the electrodes at frequencies very close to the dc limit, graphite has no influence on the frequency dependence of the conductivity beyond that frequency range. An impedance analyzer (HP 4192A LF) for the frequency range between 5 Hz and 13 MHz was used to measure the real and imaginary parts of the conductivity. The sample holder has a four-terminal configuration.

3. Nuclear magnetic resonance spectroscopy

3.1. Results

3.1.1. Glassy sample

The temperature dependence of the spin–lattice relaxation rate of the glassy sample at various frequencies is shown in Fig. 1. The rate maxima, covered in the runs at medium frequencies only, are located in the range 800 K $\leq T_{max} \leq$ 840 K. The very first points of the high-temperature sides indicate that the peaks are not symmetric in contradiction to the classical model of relaxation by Bloembergen, Purcell and Pound (BPP) [11]. This feature is well known from other ion-conducting materials [12]. The activation energies, E_{nmr}^{lT}, obtained from the slopes of the low-temperature flanks of the peaks at various frequencies scatter about 0.22 eV ± 0.02 eV without an obvious trend in the frequency dependence to be observed. Below room temperature the low-temperature flank passes into a region where relaxation is only slightly temperature dependent. This behavior is observed down to the lowest temperatures we examined (about 150 K). On the high-temperature flank there are too few data points to determine the precise value of E_{nmr}^{hT}, a lower limit being 0.3 eV.

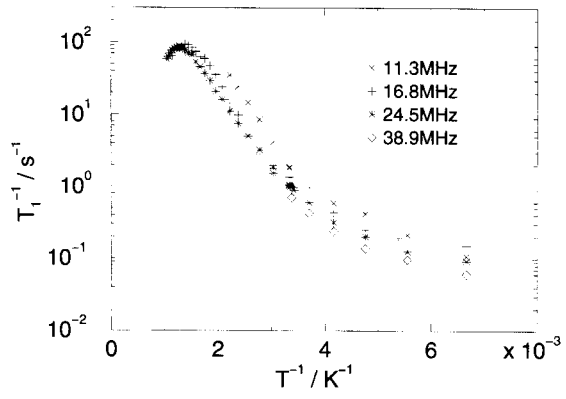

Fig. 1. Spin–lattice relaxation rate of ^7Li in glassy $LiAlSi_4O_{10}$ versus reciprocal temperature at various Larmor frequencies.

The frequency dependence of the relaxation rate data on the low-temperature flank can be described by the relation

$$T_1^{-1} \propto \nu_0^{-\alpha}. \quad (1)$$

In the present system, α was found to be 0.8 ± 0.5, which, again, is contradictory to the BPP prediction of $\alpha = 2$. A sublinear frequency dependence, as in the case of the structurally equivalent β-spodumene [5] and other oxide glasses [13], cannot unambiguously be derived from the present data due to the large experimental error.

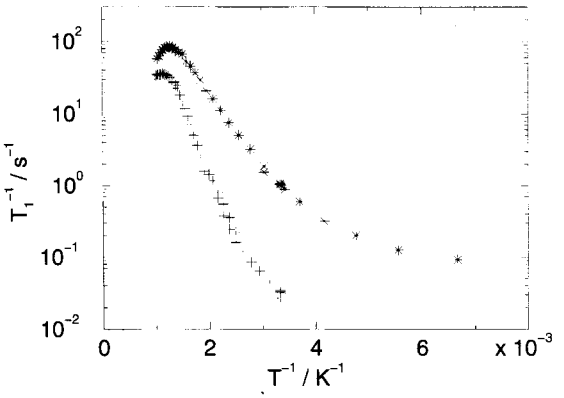

Fig. 2. Spin–lattice relaxation rates of glassy (∗) and crystalline (+) $LiAlSi_4O_{10}$ versus reciprocal temperature at $\nu_0 = 24.5$ MHz.

3.1.2. Crystalline sample

In order to compare amorphous and crystalline modifications of the same composition, spin–lattice relaxation has been investigated using a β-spodumene–SiO_2–solid solution sample having the same composition as the glassy sample. In Fig. 2 Arrhenius plots are shown for both modifications at 24.5 MHz above room temperature. The activation energy, E_{nmr}^{IT}, as calculated from the slope of the upper part of the low-temperature side, is 0.47 eV for the crystalline sample. The rate maximum appears at $T_{max} = 880$ K. Although only few data points were observed on the high-temperature side, it becomes obvious that the peak is rather broad.

3.2. Discussion

In order to determine the dominant kind of coupling of the ^{7}Li nuclear probe an estimation of the dipolar contribution to the spin–lattice relaxation rate was carried out by evaluating [14]

$$\begin{aligned} T_1^{-1} = \left(\frac{\mu_0}{4\pi}\right)^2 \{ & \tfrac{3}{2} f_{Li} \gamma_{Li}^4 \hbar^2 I(I+1) \\ & \times \left[J^{(1)}(\omega_{Li}) + J^{(2)}(2\omega_{Li}) \right] \\ & + \gamma_{Li}^2 \gamma_{Al}^2 \hbar^2 S(S+1) \\ & \times \left[\tfrac{1}{12} J^{(0)}(\omega_{Li} - \omega_{Al}) + \tfrac{3}{2} J^{(1)}(\omega_{Li}) \right. \\ & \left. + \tfrac{3}{4} J^{(2)}(\omega_{Li} + \omega_{Al}) \right] \}, \end{aligned} \tag{2}$$

where μ_0 is the permeability of vacuum, f_{Li} is the natural abundance of ^{7}Li, while γ_i and ω_i denote the respective magnetogyric ratios and precession frequencies (i.e., $\omega_{Li} = 2\pi\nu_0$) for ^{7}Li and ^{27}Al. Disregarding the other nuclei contained in the sample (i.e., ^{6}Li or ^{29}Si) does not induce a considerable error because of their small natural abundances or small magnetogyric ratios. The spectral densities J are given by

$$\begin{aligned} J^{(0)}(\omega) &= \tfrac{8}{5} \sum r^{-6} \left(\frac{\tau_c}{1 + \omega^2 \tau_c^2} \right), \\ J^{(1)}(\omega) &= \tfrac{1}{6} J^{(0)}(\omega), \\ J^{(2)}(\omega) &= \tfrac{2}{3} J^{(0)}(\omega), \end{aligned} \tag{3}$$

with τ_c being the NMR correlation time and r the distance from one ^{7}Li nucleus to another in the first term of Eq. (2) and to ^{27}Al in the second one. For the calculation, the low-temperature flank activation energy was used; the correlation time has been estimated from the relation

$$2\pi\tau_c\nu_0 \approx 1 \tag{4}$$

at the temperature of the rate maximum. The results are displayed in Fig. 3. The calculated dipolar relaxation rate is only a few percent of the total measured rate. Thus it may be concluded, considering the high purity of the sample with respect to paramagnetic ions, that the relaxation in $LiAlSi_4O_{10}$ is dominated by the interaction of the lithium nuclear quadrupole moment with local electric field gradients. Though

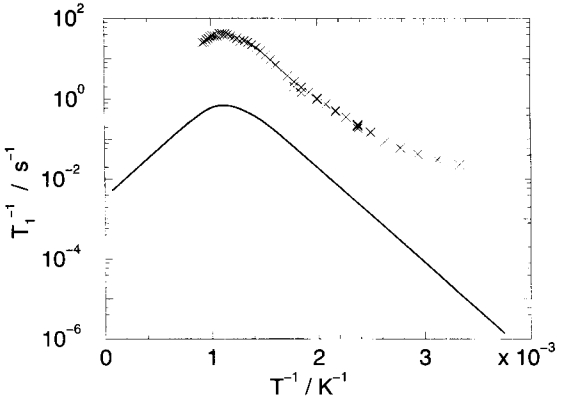

Fig. 3. Dipolar contribution to spin–lattice relaxation rate in comparison with measured overall relaxation rate for crystalline $LiAlSi_4O_{10}$ at a Larmor frequency of 24.5 MHz, displayed versus inverse temperature. The calculated values are represented by the solid line (cf. Eq. (2)); crosses indicate measured data.

the exact values for the interionic distances are known for the crystal only, we assume this estimation to be valid for the glass, too, as there will be a widespread distribution of interionic distances, but their mean value is expected to be close to the distance in the crystal.

As mentioned above, there are two indications of non-BPP behavior which are manifested in the glassy material: first, the asymmetry of the spin–lattice relaxation rate peak, and, second, the subquadratic frequency dependence of the relaxation rate on the low-temperature flank.

Relaxation theories for solid electrolytes, such as the coupling concept [15], the assumption of a distribution of correlation times [16] and the jump relaxation model [17], all predict a low-temperature flank expression for the relaxation rate given by

$$T_1^{-1} \sim \nu_0^{-\alpha} \exp\left(-\frac{E_{\mathrm{nmr}}^{\mathrm{lT}}}{kT}\right), \tag{5}$$

where α is limited by $1 \leq \alpha \leq 2$. Bunde and coworkers [18] found that this limit holds true also for the Monte Carlo simulation approach to NMR correlation functions of ionic motion in structurally disordered solids. The previously mentioned anomalies of spin–lattice relaxation are shown to be the consequence of the combined effect of structural disorder and Coulomb interactions of the moving particles, while either of these alone should result in nearly the classical BPP behavior. Structural disorder may in this context be described by the dynamic structure model [19], which was developed for glasses but may be extended to disordered crystalline materials with structural relaxation effects. Here disorder is modeled by means of a percolation approach.

According to all of these models the high- and low-temperature side activation energies are related by

$$E_{\mathrm{nmr}}^{\mathrm{lT}} = (\alpha - 1)\, E_{\mathrm{nmr}}^{\mathrm{hT}}. \tag{6}$$

Thus the parameter α links the frequency dependence of the rate (cf. Eq. (5)) to the asymmetry of the relaxation rate peak (cf. Eq. (6)). Following, for example, the jump relaxation approach, it is possible to compare spectral densities from spin–lattice relaxation time measurements, incoherent neutron scattering, and ac impedance spectroscopy, all of which contain the universal parameter α in a mathematically analogous way, provided that jump relaxation, i.e., the process of correlated jumping of defects in a solid electrolyte, is the dominating kind of motion.

The relaxation models cited above postulate an exponent α with $1 \leq \alpha \leq 2$. The possibility that $\alpha < 1$, being allowed for by the present experimental results, cannot be explained by these models. Very recently, however, a unifying modification of the jump relaxation and dynamic structure models [20] provided an explanation for a sublinear frequency dependence of the spin–lattice relaxation rate in case of ions hopping along a path of preferred sites.

By comparing the data for the two modifications (cf. Fig. 2) a significant decrease of the relaxation rate (by a factor of 5 in the vicinity of the maximum) is noted over the temperature range when changing the order state of the sample from amorphous to crystalline. Also the activation energy is found to be larger in the crystalline sample. The position of the maximum on the temperature axis is shifted towards higher temperature when the structural order of the sample is increased. This implies a smaller jump frequency of the lithium ions in the crystalline material at a given temperature near the maximum.

The last two features, i.e., the crystallinity dependence of $T_{\max}$ and $E_{\mathrm{nmr}}^{\mathrm{lT}}$, are in agreement with those observed with β-spodumene, $LiAlSi_2O_6$, in its glassy and crystalline states [5], while the dependence of the relaxation rate on the crystallinity is reverse in the cited case.

4. Impedance spectroscopy

4.1. Results

In addition to the NMR measurements the ac conductivity relaxation in the glassy sample was observed. Impedance spectra (imaginary versus real part of specific impedance) recorded at three different temperatures are shown in Fig. 4. In contrast to an ideal electrolyte (i.e., Debye-type) the spectra are shaped like depressed semicircular arcs. This deviation can be described in terms of a Cole–Cole fit [21]. For this purpose an equivalent circuit containing an Ohmic resistor and a constant phase element (CPE) in parallel is used as equivalent for the sam-

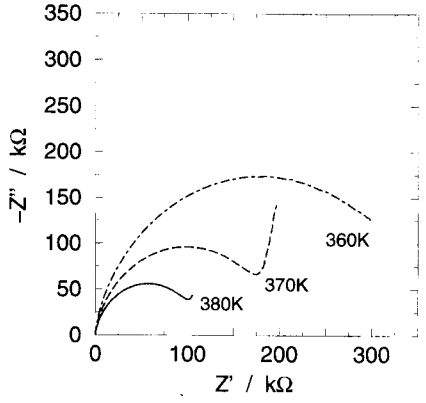

Fig. 4. Impedance spectrum of glassy $LiAlSi_4O_{10}$, at various temperatures. Both axes are displayed on the same scale. Frequency increases from right to left.

ple. The CPE is a frequency dependent capacitor and results in a complex conductivity of $\sigma^* \propto (i\omega)^m C$, with $0 \leq m \leq 1$ being the Cole–Cole exponent and C the capacitance of the CPE. In $LiAlSi_4O_{10}$ we found $m = 0.8$ without a significant temperature dependence, whereas in a Debye-type electrolyte the conductivity is not frequency dependent, i.e., $m = 0$. This non-Debye-type behavior was previously observed in other ion-conducting glasses (see, for example, Ref. [22]).

In order to obtain activation energies related to the ionic conductivity, the product of the real part of the conductivity and the temperature is displayed in an Arrhenius plot (Fig. 5). This product $\sigma'T$ is the relevant quantity when assuming an Arrhenius-type activation for the diffusivity, which is related to $\sigma'T$ by the Nernst–Einstein equation. From the frequency-independent high-temperature branch of the graph one obtains the dc activation energy $E_\sigma^{dc} = 0.68$ eV. The slope of the low temperature branch is governed by the ac activation energy E_σ^{ac} which is increasing with decreasing frequency, from 0.4 eV at 1 MHz to 0.6 eV at 1 kHz.

The frequency dependence of the conductivity can be described by a power law [23]

$$\sigma' \propto \nu^n. \tag{7}$$

The exponent n can be obtained from a plot of $\log \sigma'T$ versus $\log \nu$ (Fig. 6). The frequency range of the data shown in Fig. 6 is limited by electrode polarization at low frequencies and by the measuring range of our impedance analyzer at high frequencies. At the lowest accessible frequencies we note the curves approaching the (temperature dependent) dc limit. At the upper end of the frequency range the conductivity reaches the dispersive regime. The dispersion exponent, n, can be identified as the slope of the curves in this region. It decreases with increasing temperature from $n = 0.5$ at 320 K to $n = 0.2$ at 500 K. Thus the Debye case ($n = 0$) is approached asymptotically with increasing temperature.

An alternative way of describing IS data, proposed by Macedo et al. [24], is the modulus formalism. The electric modulus is defined by

$$M^* = M' + iM'' \propto i\omega\rho^*, \tag{8}$$

emphasizing the impedance of the sample rather than

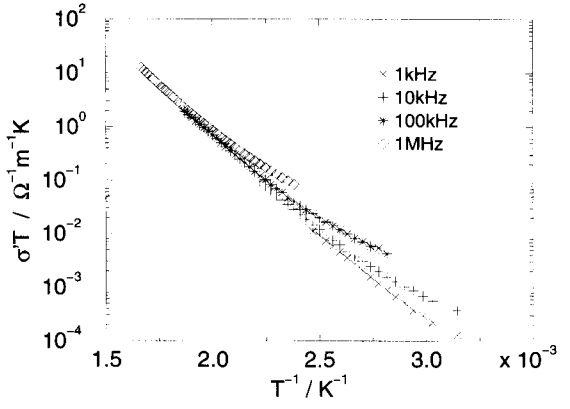

Fig. 5. Product of real part of the conductivity of glassy $LiAlSi_4O_{10}$ and temperature $\sigma'T$ versus reciprocal temperature, at various ac frequencies.

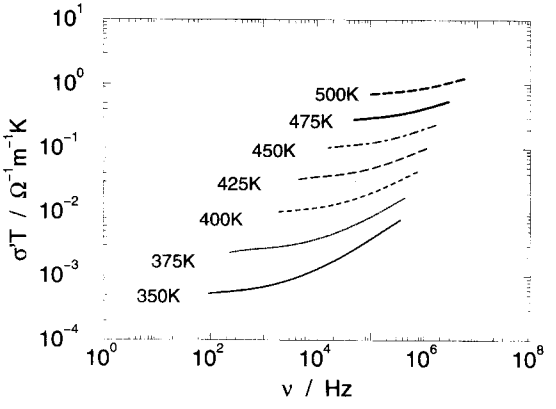

Fig. 6. Product of real part of the conductivity of glassy $LiAlSi_4O_{10}$ and temperature $\sigma'T$ versus ac frequency, at various temperatures.

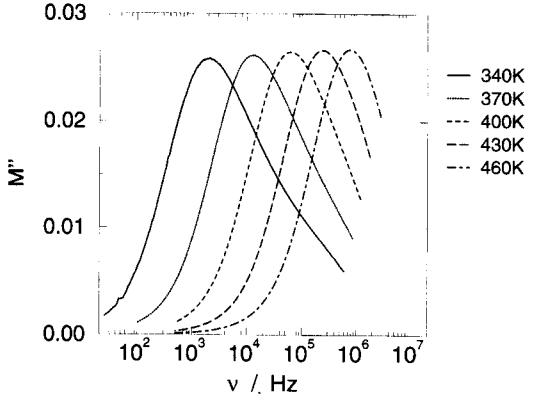

Fig. 7. Imaginary part of the electric modulus of glassy $LiAlSi_4O_{10}$ versus ac frequency.

its conductivity. When plotting the imaginary part of the modulus versus log frequency (Fig. 7), the full width at half maximum (FWHM) of the peak can be evaluated up to 430 K. At higher temperatures, only part of the peak is covered within the frequency range of the experimental setup. An anomaly can also be observed with the electric modulus: The FWHM is greater than the 1.14 decades that are predicted by the Debye theory. We found the FWHM of the peak to decrease with increasing temperature from 2.5 decades at 340 K to 1.9 decades at 430 K. Thus the trend of approaching ideal behavior with rising temperature which was observed within the conductivity formalism is recovered within the modulus formalism.

4.2. Discussion

As observed with the NMR results, the Li^+ diffusion-induced relaxation of ^7Li in $LiAlSi_4O_{10}$ deviates clearly from the standard model. Similarly the impedance results also deviate from the Debye model. The non-Debye type behavior reveals itself by (i) the fact that the impedance spectra consist of depressed semicircular arcs, (ii) the dispersion of the conductivity, and (iii) the broadening of the modulus peak in the frequency dependent plot.

In an attempt to quantify this non-ideality, Kanert et al. [25] suggested consideration of the coupling parameter, n_σ (and, analogously, n_s for spin–lattice relaxation), which can be calculated from the frequency dependence of $\sigma'T$ as well as M'' at low temperatures. In the case of conductivity relaxation this approach leads to the well-known power law (cf. Eq. (7)). In the coupling concept, the activation energies from the low-temperature branches of the Arrhenius plots of $\sigma'T$ and M'' are interpreted in terms of a microscopic energy barrier, $\overline{E}$. From the equation

$$E_\sigma^{dc} = \frac{\overline{E}}{1 - n_\sigma}, \tag{9}$$

the coupling parameter, n_σ, can be extracted. For frequencies below about 1 MHz its value scatters slightly about 0.7.

A more pictorial interpretation of the data can be achieved using the dynamic structure model [26]. The authors describe disorder in an ionic conductor by means of a percolation approach, i.e., several sites are inaccessible for the mobile species. If there are comparatively large regions of such forbidden sites, mobile ions will be trapped at the surface of these regions, where they build up a strong local electrical field together with the fixed surface anions. This trapping results in shorter interatomic distances as compared to freely mobile ions in those parts of the bulk that consist only of accessible sites. Apart from that, the ions are less mobile in these trapping regions at the surfaces of the inaccessible regions than in the bulk material due to the local enhancement of the electric field. Within this concept of classifying the charge carriers as mobile and less mobile ions, the broadening of the modulus peak (Fig. 7) may be assigned to a distribution of such inaccessible regions of different size, with differing surface charge densities. Thus, their ability to trap mobile ions differ and this model can be represented by a series of several RC elements (elements containing an ohmic resistor and a capacitor in parallel, cf. [27]).

Tatsumisago et al. [28] proposed to extract from the maximum of the modulus peak the so-called conductivity relaxation time, τ_σ, defined by

$$\tau_\sigma = (2\pi\nu_{max})^{-1}. \tag{10}$$

The values of τ_σ in the present system range from 1×10^{-8} s at 580 K to 3×10^{-4} s at 320 K. It has been suggested [17] that the frequency which indicates the crossover from the dc plateau to the dispersive regime of the ionic conductivity may be used as

a measure for the hopping frequency of the mobile charge carriers. The corresponding time constant, t_1, as obtained from this crossover in Fig. 6, yields values of the same order of magnitude as τ_σ, e.g., $t_1 = 2 \times 10^{-4}$ s at 350 K.

5. Comparison of NMR and IS results

5.1. Presentation of IS data in a form comparable to NMR data

In order to compare NMR and IS results Munro et al. [3] suggested the use of the specific impedance instead of the specific conductivity as a basis for the Arrhenius plot leading to the frequency dependent activation energies. This method is equivalent to switching from the conductivity to the modulus formalism, because the real part of the specific resistivity, ρ', is proportional to M''/ω and dependent on τ_σ

$$\rho' \propto \frac{\tau_\sigma}{1 + (\omega\tau_\sigma)^2}. \tag{11}$$

As $\tau_\sigma \propto \log(1/T)$ [24], this implies that $\log \rho'$ versus T^{-1} is a peaked function. Thus it has, in analogy to the NMR Arrhenius plots, a low- and a high-temperature side — each of which yield an activation energy, E_ρ^{lT} and E_ρ^{hT}, respectively, that may be compared to the corresponding NMR quantities $E_{\mathrm{nmr}}^{\mathrm{lT}}$ and $E_{\mathrm{nmr}}^{\mathrm{hT}}$. (In [3], E_ρ^{lT} is named apparent activation energy, $E_{\mathrm{a}}^{\mathrm{app}}$.) An ideal Debye-type electrolyte is expected to show a symmetric peak; and the activation energies E_ρ^{lT}, E_ρ^{hT}, $E_{\mathrm{nmr}}^{\mathrm{lT}}$, and $E_{\mathrm{nmr}}^{\mathrm{hT}}$ should have a common value. Deviations from Debye-type behavior — which at the same time means deviations from BPP-type behavior in NMR relaxation — will result in different slopes of the high- and low-temperature sides of each of the two functions, $\log \rho'(T^{-1})$ and $\log T_1^{-1}(T^{-1})$. Furthermore the high-temperature slopes of both functions are expected to remain identical, having the dc value. In glassy $LiAlSi_4O_{10}$ (cf. Fig. 8), we found this non-Debye type of relaxation. The activation energies E_ρ^{lT} of the low-temperature side scatter slightly about 0.2 eV, while the high temperature value E_ρ^{hT} is 0.68 eV. The low-temperature activation energies have no significant trend with frequency. Their mean value is in good agreement with $E_{\mathrm{nmr}}^{\mathrm{lT}}$ from NMR relaxation (cf. Section 3.1). On the-high temperature side of the $\rho'(T^{-1})$ peak, the dc activation energy is recovered.

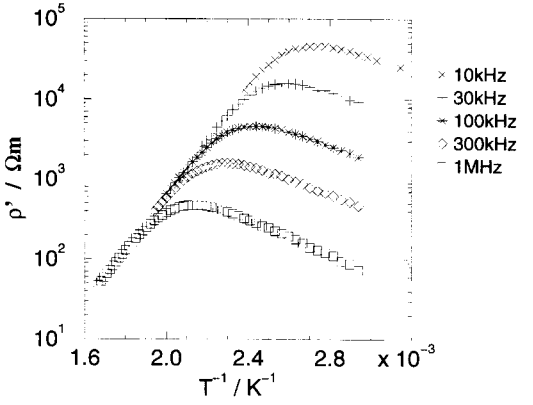

Fig. 8. Real part of the resistivity of glassy $LiAlSi_4O_{10}$ versus reciprocal temperature.

5.2. Arrhenius plots and activation energies from NMR and IS

In the context of our measurements we present three different types of Arrhenius plots: besides the spin–lattice relaxation rate (cf. Figs. 1 and 2) there are the conductivity (cf. Fig. 5) and resistivity (cf. Fig. 8) versus inverse temperature plots. Each of these in principle yields two different activation energies. From NMR relaxation one gains $E_{\mathrm{nmr}}^{\mathrm{lT}}$ and $E_{\mathrm{nmr}}^{\mathrm{hT}}$; from conductivity E_σ^{ac} can be obtained from the dispersive region and E_σ^{dc} from the non-dispersive region; and from resistivity one gets E_ρ^{hT} from the high- and E_ρ^{lT} from the low-temperature flank.

According to Funke [17] E_σ^{dc}, $E_{\mathrm{nmr}}^{\mathrm{hT}}$, and in our opinion E_ρ^{hT} as well should have the same value because they are affected by the same long-range motional process. As far as the impedance results are concerned this expectation is fulfilled: the values of the activation energies are 0.68 eV. The lack of NMR high-temperature data only permits an estimation of a lower limit for $E_{\mathrm{nmr}}^{\mathrm{hT}} = 0.3$ eV, which supports the above expectation.

The resistivity approach, being introduced in order to obtain a representation directly comparable to

NMR Arrhenius plots, leads to values of E_ρ^{IT} about 0.2 eV. Although these data have been recorded in another frequency range than the NMR data, the comparison with E_{nmr}^{IT} shows best the similarity of the NMR and impedance approaches to ionic motion. This similarity is supported by the fact that the NMR frequency dependence, if any, is rather small.

5.3. NMR correlation and IS relaxation times

Another means of comparing the results obtained by NMR and impedance spectroscopy is displaying the temperature dependence of the NMR correlation, τ_c, and the conductivity relaxation times, τ_σ [28]. τ_c is obtained from the peak of $\log T_1^{-1}(T^{-1})$ for every single Larmor frequency ν_0 (cf. Eq. (4)), while τ_σ is extracted from the peak of $M''(\log \nu)$ for each temperature (cf. Eq. (10)). According to the higher frequencies covered by the present NMR measurements as compared to IS the τ_cs have been determined at higher temperatures. The correlation times are about 1.5 orders of magnitude larger than the extrapolated conductivity relaxation times in this temperature range. This feature is well-known from other glassy systems [3,25,28,29]. An explanation for the difference between the observations made by NMR and those from impedance measurements can be given in terms of the different correlation functions the two methods are based upon: The effects seen by NMR spectroscopy are based on space correlations. Thus ions with short distances from the probe nucleus are dominating the observed relaxation process. On the other hand, impedance spectroscopy is sensitive to velocity autocorrelations and, as these are related to the mean square displacement, consequently the contribution of fast ions is larger. In the context of the dynamic structure model this means that NMR is dominated by the comparatively slow nuclei trapped at the surfaces of inaccessible regions, while IS is influenced by mobile ions in the bulk.

Instead of τ_σ which is closely related to σ_{dc} [30], the crossover time, t_1 (cf. Section 4.2), being identified as the inverse of the hopping frequency, may be used for comparison with the NMR correlation time τ_c. Nevertheless, the above conclusions regarding the correlation times apply to this quantity as well. Within our data, t_1 can only be extracted for the lowest temperatures because of the restricted coverage of the dispersive branch of the conductivity spectra (cf. Fig. 6). However, at low temperatures, t_1 and τ_σ are of the same order of magnitude.

6. Conclusions

Spin–lattice relaxation times of glassy and polycrystalline $LiAlSi_4O_{10}$ at temperatures 150 K $< T <$ 1000 K and for five resonance frequencies within the range 11.3 MHz $< \nu_0 <$ 38.9 MHz proved to be mainly quadrupolar. The activation energies from the low- and high-temperature flanks of an Arrhenius plot of the spin–lattice relaxation rates differ; the high-temperature slope is considerably steeper. The frequency dependence of the rate on the low-temperature flank was examined for the glassy sample and can be described by a power law (cf. Eq. (1)) with an exponent $\alpha \approx 0.8$. With increasing degree of structural order (which means comparing amorphous and crystalline material) the activation energy increases and the jump frequency decreases.

Conductivity measurements at temperatures 298 K $< T <$ 670 K and frequencies 100 Hz $< \nu <$ 10 MHz show a frequency dependence with an exponent $0.2 < n < 0.5$ declining with increasing temperature. Also, the peak of the modulus, plotted versus log frequency, exhibits an anomalous width of more than 1.8 decades.

Both methods show deviations of the ionic motion in the studied materials from the standard models (BPP for spin–lattice relaxation and Debye for conductivity relaxation). Other models that are specifically constructed to explain correlated motion processes (jump-relaxation, dynamic structure, and coupling models) explain part of the results, such as the asymmetry of the relaxation rate peak and the anomalous width and shape of the modulus peak. However, they do not explain a possible sublinear frequency dependence of T_1^{-1}.

In the context of the dynamic structure model, we assumed that there are certain regions in a sample where mobile ions are trapped, so that they are less mobile than those lithium ions that can move freely in the matrix. This assumption is corroborated by the fact that an equivalent circuit containing more than two Debye-type RC elements is necessary to repre-

sent the broad modulus peak of the glassy sample. Hence in a glass there is a distribution of different-sized clusters, each of which corresponds to a different RC component.

The difference between NMR correlation times and conductivity relaxation times, extrapolated to the temperatures of the NMR relaxation rate maxima, is due to the fact that the correlation function of NMR spectroscopy samples short-range environment of the probe nuclei and the correlation funcion of IS is sensistive to fast moving ions.

Acknowledgements

We thank Dr P. Naß, Schott Glaswerke, Mainz, for providing the glassy material and Dr G. Wolff and H. Nickel from the Zentralabteilung für chemische Analysen, Forschungszentrum Jülich GmbH, for the chemical analysis of the glass. We wish to thank Dr S.H. Chung, now National Institute for Research in Inorganic Materials, Tsukuba, Japan, and Dr G. Balzer, Institut für Anorganische Chemie, Universität Hannover, for helpful discussions. Financial support by the Deutsche Forschungsgemeinschaft (SFB 173) and the Fonds der Chemischen Industrie is gratefully acknowledged.

References

[1] W. Pannhorst, R. Haug, E. Rodek and K. Stetter, J. Non-Cryst. Solids 131—133 (1991) 488.
[2] G. Roth and H. Böhm, Solid State Ionics 22 (1987) 253.
[3] B. Munro, M. Schrader and P. Heitjans, Ber. Bunsenges. Phys. Chem. 96 (1992) 1718.
[4] C.T. Li and D.R. Peacor, Z. Kristallogr. 126 (1968) 46.
[5] W. Franke and P. Heitjans, Ber. Bunsenges. Phys. Chem. 96 (1992) 1674.
[6] P. Lunkenheimer, G. Gerhard, F. Drexler, R. Böhmer, A. Loidl and W. Pannhorst, Z. Naturforsch. 50a (1995) 1151.
[7] W. Ostertag, G.R. Fischer and J.P. Williams, J. Am. Ceram. Soc. 51 (1968) 651.
[8] H.S. Chen and C.E. Miller, Rev. Sci. Instrum. 41 (1970) 1273.
[9] Yu.N. Kondratev and N.V. Chernysh, Izv. Akad. Nauk. SSSR, Neorg. Mater. 2 (1966) 1630.
[10] J. Stein, dissertation, Universität Hannover (1994).
[11] N. Bloembergen, E.M. Purcell and R.V. Pound, Phys. Rev. 73 (1948) 679.
[12] D. Brinkmann, Magn. Reson. Rev. 14 (1989) 101.
[13] G. Balzer-Jöllenbeck, O. Kanert, H. Jain and K.L. Ngai, Phys. Rev. B39 (1989) 6071.
[14] A. Abragam, The Principles of Nuclear Magnetism (Clarendon, Oxford, 1961).
[15] K.L. Ngai and O. Kanert, Solid State Ionics 53–56 (1992) 936.
[16] E. Göbel, W. Müller-Warmuth, H. Olyschläger and H. Dutz, J. Magn. Reson. 36 (1979) 371.
[17] K. Funke, Progr. Solid State Chem. 22 (1993) 111.
[18] M. Meyer, P. Maass and A. Bunde, Phys. Rev. Lett. 71 (1993) 573.
[19] A. Bunde and P. Maass, Physica A200 (1993) 80.
[20] C. Cramer, K. Funke, T. Saatkamp, D. Wilmer and M.D. Ingram, Z. Naturforsch. 50a (1995) 613.
[21] J.R. Macdonald, ed., Impedance Spectroscopy (Wiley, New York, 1988).
[22] H. Kahnt, Ber. Bunsenges. Phys. Chem. 95 (1991) 1021.
[23] A.K. Jonscher, Phys. Thin Films 2 (1964) 205.
[24] P.B. Macedo, C.T. Moynihan and R. Bose, Phys. Chem. Glasses 13 (1972) 171.
[25] O. Kanert, R. Küchler, K.L. Ngai and H. Jain, Phys. Rev. B49 (1994) 76.
[26] M. Meyer, P. Maass and A. Bunde, J. Non-Cryst. Solids 172–174 (1994) 1292.
[27] I.M. Hodge, M.D. Ingram and A.R. West, J. Electroanal. Chem. 74 (1976) 125.
[28] M. Tatsumisago, C.A. Angell and S.W. Martin, J. Chem. Phys. 97 (1992) 6968.
[29] W. Franke, P. Heitjans, B. Munro and M. Schrader, in: Defects in Insulating Materials, ed. O. Kanert and J.M. Spaeth (World Scientific, Singapore, 1993) p. 1009.
[30] C.A. Angell, Ann. Rev. Phys. Chem. 43 (1992) 693.